

RECENT ADVANCES IN GRAVITATIONAL LENSING

Y. Mellier^(1,4), L. Van Waerbeke⁽²⁾, F. Bernardeau⁽³⁾, B. Fort⁽⁴⁾

⁽¹⁾*Institut d'Astrophysique de Paris,
98^{bis} Boulevard Arago,
75014 Paris, France.*

⁽²⁾*Observatoire Midi Pyrénées,
14 Av. Edouard Belin,
31400 Toulouse, France.*

⁽³⁾*Service Physique Théorique,
CE de Saclay,
91191 Gif-sur-Yvette Cedex, France.*

⁽⁴⁾*Observatoire de Paris (DEMIRM),
61 Av. de l'Observatoire,
75014 Paris, France.*

Abstract

The gravitational lensing effect is one of the most promising tools for cosmology. Indeed it probes directly the total mass distribution in large-scale structures and can as well provide valuable informations on the values of the density parameter Ω and the cosmological constant λ . In this review we summarize the most spectacular observational and theoretical advances obtained in this field during the last five years.

1 Introduction

The observed structures of the universe are thought to originate from the gravitational condensation of primordial mass-energy fluctuations whose evolution depends on the power spectrum of the initial fluctuations, the amount and nature of the various matter components present in the early universe and the eventual existence of a cosmological constant. Since most of the acting gravitational masses remain invisible, constraining cosmological scenario from astronomical observations has been one of the most fascinating challenge of the last decades. From the observations of the spatial galaxy distribution (see de Lapparent, this conference), and from dynamical studies of gravitational systems like galaxies or clusters of galaxies, it is possible to infer the amount of dark matter as well as its distribution, or to have insights into the clustering properties of the visible matter in the universe. However, none of these observations measures *directly* the total amount and the distribution of matter: angular or redshift surveys give the distribution of *light* associated with galaxies, and mass estimations of gravitational structures can only be obtained within the assumption that they are simple relaxed or virialised dynamical systems. Dynamics of galaxy velocity fields seems an efficient and promising approach to map directly the potentials responsible from large-scale flows, but catalogs are still poor and some assumptions are still uncertain or poorly understood on a physical basis.

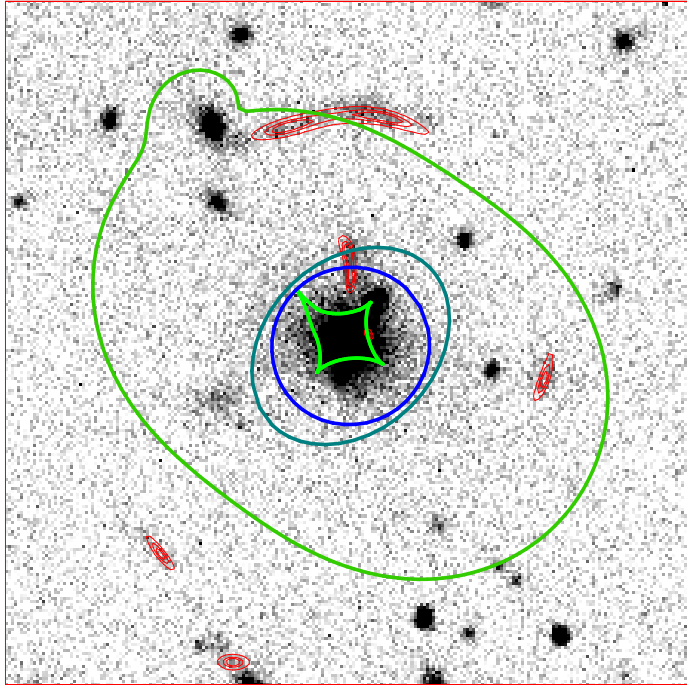


Figure 1: Model of MS2137-23. This cluster is at redshift 0.33 and shows a tangential arc and the first radial arc ever detected. Up to now it is the most constrained cluster and the first one where counter images were predicted before being observed (Mellier et al. 1993). The external and the dark internal solid lines are the critical lines. The internal grey ellipse and the diamond are the caustic lines. The thin isocontours shows the positions of the arcs and their counter images.

Gravitational lensing effects are fortunately a direct probe of deflecting masses in the universe. They allow to determine directly the amount of matter present along the line-of-sight from observed or reconstructed deflection angles. After the discovery of the first multiply imaged quasar (Walsh et al. 1979) and the first observations of gravitational arcs (Soucail et al. 1987, 1988; Lynds & Petrossian 1986) and arclets (Fort et al. 1988), gravitational lensing rapidly becomes one of the most useful tool for probing dark matter on all scales and cosmological parameter as well. In the following, we summarize what we have learned from strong and weak lensing regimes in clusters of galaxies and how constraints on the cosmological parameters can, or could, be obtained. We will also discuss a technique for measuring gravitational shear that has been developed recently and which opens new perspectives for the observations and the analysis of lensing effect by large-scale structures, as those we discuss in the last section.

2 Definitions and lensing equations

Let us remind the basic principles of the gravitational lensing effects. A deflecting mass changes the apparent position of a source $\vec{\theta}_S$ into the apparent image position $\vec{\theta}_I$ by the quantity $\vec{\alpha}$:

$$\vec{\theta}_S = \vec{\theta}_I + \vec{\alpha}(\vec{\theta}_I) . \quad (1)$$

The deflection angle $\vec{\alpha}(\vec{\theta}_I)$ is the gradient of the two-dimensional (projected along the line of sight at the angular position $\vec{\theta}_I$) gravitational potential ϕ . The gravitational distortion of background objects is described by the Jacobian of the transformation, namely the amplification matrix \mathcal{A} between the source and the image plane (Schneider, Ehlers & Falco 1992):

$$\mathcal{A} = \begin{pmatrix} 1 - \kappa - \gamma_1 & -\gamma_2 \\ -\gamma_2 & 1 - \kappa + \gamma_1 \end{pmatrix}, \quad (2)$$

where κ is the convergence, γ_1 and γ_2 are the shear components. They are related to the Newtonian gravitational potential ϕ by:

$$\kappa = \frac{1}{2} \nabla^2 \phi = \frac{\Sigma}{\Sigma_{\text{crit.}}}; \quad \gamma_1 = \frac{1}{2} (\phi_{,11} - \phi_{,22}); \quad \gamma_2 = \phi_{,12}, \quad (3)$$

where Σ is the projected mass density and $\Sigma_{\text{crit.}}$ is the critical mass density which would exactly focus a light beam originating from the source on the observer plane. It depends on the angular diameter distances D_{ab} , (where $a, b = [o(bserver), l(ens)ors(ource)]$) involved in the lens configuration:

$$\Sigma_{\text{crit.}} = \frac{c^2}{4\pi G} \frac{D_{os}}{D_{ol} D_{ls}}. \quad (4)$$

Depending on the ratio $l = \Sigma/\Sigma_{\text{crit.}}$ we most often distinguish for data analysis the strong lensing ($l \gtrsim 1$) and the weak lensing ($l \ll 1$) regimes. Note that the values of the cosmological parameters enter in the relationship between the angular distance and the redshift. This is this dependence that, in some cases, can be used to constrain Ω or λ .

3 Arcs and mass in the central region of clusters of galaxies

Arcs and arclets correspond to strong lensing cases with $l \gg 1$ and $l \approx 1$ respectively. Giant arcs form at the points where the determinant of the magnification matrix is (close to) infinite. To these points (the critical lines) correspond the caustic lines in the source plane. From the position of the source with respect to the caustic line, one can easily define typical lensing configuration with formation of giant arcs from the merging of two or three images, or radial arcs and “straight arc” as well (see Fort & Mellier 1994, Narayan & Bartelmann 1996).

Some of these typical lensing cases have been observed in rich clusters of galaxies. For MS2137-23 (Mellier et al. 1993; see figure 1), A370 (Kneib et al. 1993), Cl0024+1654 (Wallington et al. 1995), A2218 (Kneib et al. 1995), very accurate models with image predictions have been done which provide among the most precise informations we have about the central condensation of dark matter of clusters of galaxies on scale of $\approx 300h^{-1}\text{kpc}$ (table 1). In particular, giant arcs definitely demonstrate that clusters of galaxies are dominated by dark matter, with mass-to-light ratio (M/L) larger than 100, which closely follows the geometry of the diffuse light distribution associated with the brightest cluster members. Furthermore, since arcs occur when $\Sigma/\Sigma_{\text{crit.}} \gg 1$, clusters of galaxies must be much more concentrated, e.g. with a smaller core radius, than it was expected from their galaxy and X-ray gas distributions. Note that the occurrence of arcs is also enhanced by the existence of additional clumps observed in most of rich clusters which increases the shear substantially (Bartelmann 1995). The direct observations of substructures by using giant arcs confirm that clusters are dynamically young systems, therefore pointing towards a rather high value of Ω .

| CLUSTER | Z | SCALE | M/L | Z(ARC) | CLUSTER TYPE | REF. |
|-----------|------|---------|----------|-------------|--------------|------------------------|
| MS2137 | 0.33 | 500 Kpc | 340-140h | 0.70 - 1.5 | SIMPLE | Mellier et al. 1993 |
| A370 | 0.37 | 500 Kpc | >150h | 0.72 | BIMODAL | Kneib et al. 1993 |
| Cl0024+17 | 0.39 | 500 Kpc | >200h | 0.90 | SIMPLE | Kassiola et al. 1992 |
| Cl0024+17 | 0.39 | 2.5 Mpc | >200h | 0.90 | SIMPLE | Wallington et al. 1995 |
| A2218 | 0.18 | 1.0 Mpc | 200h | 0.7 and 1.3 | BIMODAL | Kneib et al. 1995 |
| A2390 | 0.23 | 400 Kpc | 250h | 0.91 | BIMODAL | Pierre et al. 1996 |

Table 1: Summary of mass from giant arcs. We only give some typical examples. More details can be found in Fort & Mellier (1994) and Narayan & Bartelmann (1996). The scales are expressed in h_{100}^{-1} Kpc.

4 The weak lensing regime and lensing inversion in clusters

4.1 Lensing inversion and mass reconstruction

Beyond the region of strong lensing, background galaxies are still weakly magnified. The light deviation induces a small increase of their ellipticity in the direction perpendicular to the gradient of the projected potential (shear). Despite the intrinsic ellipticity of the sources and some observational or instrumental effects it is possible to make statistical analysis of this coherent polarization of the images of background galaxies and to recover the mass distribution of the lens. These weakly distorted galaxies are like a background distorted grid which can be used to probe the projected mass density Σ of the foreground lens. The shape parameters of the images M^I are related to the shape parameters of the sources M^S by the equation,

$$M^S = \mathcal{A}M^I\mathcal{A}, \quad (5)$$

where M are the second order momenta of objects and \mathcal{A} the magnification matrix. We thus have a relation between the ellipticity of the sources $\vec{\epsilon}_S$ and the observed ellipticity of the images $\vec{\epsilon}_I$:

$$\vec{\epsilon}_S = \frac{\vec{\epsilon}_I - \vec{g}}{1 - \vec{g} \cdot \vec{\epsilon}_I}; \quad \vec{g} = \frac{\vec{\gamma}}{1 - \kappa}. \quad (6)$$

In particular, if the sources are randomly distributed then their averaged intrinsic ellipticity verifies $\langle \vec{\epsilon}_S \rangle = 0$ and we have

$$\vec{g} = \langle \vec{\epsilon}_I \rangle. \quad (7)$$

Since the main domain of application of the weak lensing is the large-scale distribution of the Dark Matter, at scale above $> 0.5 h^{-1}$ Mpc, the analysis has been mainly focussed on the weak lensing regime, where $(\kappa, \gamma) \ll 1$. The relations between the physical ($\vec{\gamma}$) and observable ($\vec{\epsilon}_I$) quantities are then simpler, since we have,

$$\langle \vec{\epsilon}_I \rangle = \vec{\gamma}. \quad (8)$$

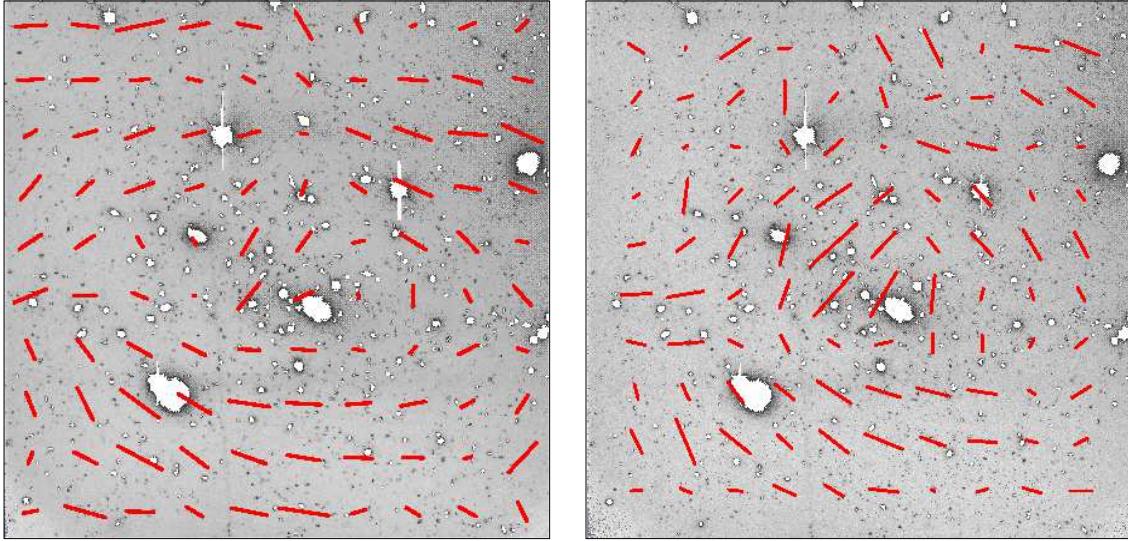


Figure 2: Shear maps around the rich lensing cluster A1942. The CCD images is a 4 hours exposure obtained at the Canada-France-Hawaii Telescope in excellent seeing conditions ($0.65''$). North is top and east is on the left. On the left panel, the shear is measured by using the Bonnet & Mellier's method which consists in computing shape parameters of an annular aperture centered of each individual galaxies. On the right panel, the shear is obtained by computing the autocorrelation (ACF) of the images (see section 4.2). Though the shape is almost the same, the signal to noise is higher with the ACF. Note the central pattern which shows the bimodal nature of the mass distribution located on the two brightest cluster members, and the eastern extension of the shear pattern probably due to a substructure.

The projected mass density Σ of the lens can be obtained from the distortion field by using Eq.(8) and the integration of Eq. (3) (Kaiser & Squires 1993):

$$\kappa(\vec{\theta}_I) = \frac{-2}{\pi} \int d^2\vec{\theta} \frac{\vec{\chi}(\vec{\theta} - \vec{\theta}_I)}{(\vec{\theta} - \vec{\theta}_I)^2} \cdot \vec{\gamma}(\vec{\theta}_I) + \kappa_0 ; \quad \vec{\chi}(\vec{\theta}) = \left(\frac{\theta_1^2 - \theta_2^2}{\theta^2}, \frac{2\theta_1\theta_2}{\theta^2} \right), \quad (9)$$

where κ_0 is the integration constant. In the weak lensing regime, Eqs.(9) provides a mapping of the total projected mass, using the distortion of the background objects.

Several improvements of the basic theory of lensing inversion have been discussed in details by Seitz & Schneider (1995, 1996), Schneider (1995) and Kaiser (1996). Note that the objects are also magnified by a factor μ which, in case of the weak lensing regime, has the form,

$$\mu = 1 + 2\kappa . \quad (10)$$

This gives potentially another independent way to measure the projected mass density Σ of a lens using the magnification instead of the distortion.

Table 2 gives a summary of the clusters for which lensing inversion have been attempted. When compare with mass distribution inferred from strong lensing, there is a clear trend towards higher M/L when the scale increases. Bonnet et al. (1994) found M/L close to 600 at $2.5 h^{-1}\text{Mpc}$ from the cluster center. Note also the remarkable results from Kaiser & Luppino on a cluster at redshift 0.83, for which the estimated mass strongly depends on the redshifts of the sources. Indeed in general the estimation of the cluster mass using Eq. (9) requires the knowledge of $\Sigma_{\text{crit.}}$, which depends on the usually poorly known redshifts of the sources. Though this is not a critical issue for nearby clusters ($z_l < 0.2$), because then $D_{os}/D_{ls} \simeq 1$, it could lead to large mass uncertainties for more distant clusters it is the case for MS1054.

| CLUSTER | Z | SCALE | M/L | Z(SOURCE) | REF. |
|-----------|------|---------|-----------------------|---------------------------------------|-----------------------|
| 1455+22 | 0.26 | 500 Kpc | 460h | | Smail et al. 1994 |
| Cl0016+16 | 0.55 | 500 Kpc | 430h | | Smail et al. 1994 |
| MS1224 | 0.33 | 500 Kpc | 800h | 1.0 -- 2.0 | Fahlman et al. 1994 |
| Cl0024+17 | 0.39 | 2.5 Mpc | 600h | 0.9 -- 1.2 | Bonnet et al. 1994 |
| A1689 | 0.18 | 1.0 Mpc | 400h | 1.0 -- 2.0 | Tyson & Fischer 1995 |
| A2218 | 0.18 | 400 Kpc | 440h | 1.0 -- 2.0 | Squires et al. 1996a |
| A2390 | 0.23 | 1 Mpc | 320h | 1.0 -- 2.0 | Squires et al. 1996b |
| MS1054 | 0.83 | 1.9 Mpc | 1600h 580h 350h | IF IF IF z<1 z=1.5 z=3 | Luppino & Kaiser 1996 |
| A1689 | 0.18 | 500 Kpc | >200h | 1.0 -- 2.0 | Broadhurst 1996 |
| A1689 | 0.18 | 1 Mpc | 400h | 1.0 -- 2.0 | Kaiser 1996 |
| Cl0939 | 0.41 | 400 Kpc | 200h | 0.6 -- 1.0 | Seitz et al. 1996 |

Table 2: Summary mass obtained from weak lensing inversion in the literature. The averaged mass-to-light ratio is higher than the one inferred from giant arc (see table 1) which is interpreted as a real increase with distance from the cluster center. Note the strong uncertainty in the case of MS1054 which is due to the strong dependence of mass with the redshift of sources as the redshift of the lens increases. The scales are expressed in h_{100}^{-1} Kpc.

Actually, even if the redshift of the sources were known, it would still not be possible to get the absolute value of the mass distribution, because possible mass planes of constant density intercepting the line of sight do not change the shear map. Mathematically, this corresponds to the unknown integration constant κ_0 in Eq.(10). This degeneracy may be broken if one measures the magnification μ which depends on the mass quantity inside the light beam (Eq.(3)). While the shear measurement does not require any information in the source plane, the magnification measurement needs the observation of a reference (unlensed) field to calibrate the magnification. Broadhurst et al. (1995) proposed to compare the number count $N(m, z)$ and/or $N(m)$ in a lensed and an unlensed field to measure μ . Depending on the value of the slope S of the number count in the reference field, we observe a bias (more objects) or an anti-bias (less objects) in the lensed field. The particular value $S = 0.4$ corresponds to the case where the magnification of faint objects is exactly compensated by the dilution of the number count (Eq.(18)). This method was applied on the cluster A1689 (Broadhurst, 1995), but the signal to noise of the detection remains 5 times lower than with the distortion method for a given number of galaxies. The magnification may also be determined by the changes of the image sizes at fixed surface brightness (Bartelmann & Narayan 1995).

The difficulty with these methods is that they required to measure the shape, size and magnitude of very faint objects up to B=28 which depends on the detection threshold, the convolution mask and the local statistical properties of the noise. These remarks led us to

propose a new method to analyze the weak lensing effects, based on the auto-correlation function of the pixels in CCD images, which avoids shape parameter measurements of individual galaxies (Van Waerbeke et al. 1996a). It is described in the next subsection.

4.2 The Auto-correlation method

The CCD image is viewed as a density field rather than an image containing delimited objects. The surface brightness, $I(\vec{\theta})$, in the image plane in the direction $\vec{\theta}$ is related to the surface brightness in the source plane $I^{(s)}$ by the relation,

$$I(\vec{\theta}) = I^{(s)}(\mathcal{A}\vec{\theta}), \quad (11)$$

which can be straightforwardly extended to the auto-correlation function (ACF) (e.g. the two-point autocorrelation function of the light distribution in a given area),

$$\xi(\vec{\theta}) = \xi^{(s)}(\mathcal{A}\vec{\theta}). \quad (12)$$

This equation is more meaningful when it is written in the weak lensing regime,

$$\xi(\vec{\theta}) = \xi^{(s)}(\theta) - \theta \partial_\theta \xi^{(s)}(\theta)[1 - \mathcal{A}] \quad (13)$$

since the local ACF, $\xi(\vec{\theta})$, now writes as the sum of an isotropic unlensed term, $\xi^{(s)}(\theta)$, an isotropic lens term which depends on κ , and an anisotropic term which depends on γ_i .

Let us now explore the gravitational lensing information that can be extracted from the shape matrix \mathcal{M} of the ACF,

$$\mathcal{M}_{ij} = \frac{\int d^2\theta \xi(\vec{\theta}) \theta_i \theta_j}{\int d^2\theta \xi(\vec{\theta})}. \quad (14)$$

The shape matrix in the image plane is simply related to the shape matrix in the source plane $\mathcal{M}^{(s)}$ by $\mathcal{M}_{ij} = \mathcal{A}_{ik}^{-1} \mathcal{A}_{jl}^{-1} \mathcal{M}_{kl}^{(s)}$. If the galaxies are isotropically distributed in the source plane, $\xi^{(s)}$ is isotropic, and in that case $\mathcal{M}_{ij}^{(s)} = M \delta_{ij}$, where δ_{ij} is the identity matrix. Using the expression of the amplification matrix \mathcal{A} we get the general form for \mathcal{M} ,

$$\mathcal{M} = \frac{M(a + |g|^2)}{(1 - \kappa)^2(1 - |g|^2)} \begin{pmatrix} 1 + \delta_1 & \delta_2 \\ \delta_2 & 1 - \delta_1 \end{pmatrix}. \quad (15)$$

The observable quantities (distortion δ_i and magnification μ) are given in terms of the components of the shape matrix,

$$\delta_1 = \frac{\mathcal{M}_{11} - \mathcal{M}_{22}}{\text{tr}(\mathcal{M})}; \quad \delta_2 = \frac{2\mathcal{M}_{12}}{\text{tr}(\mathcal{M})}; \quad \mu = \sqrt{\frac{\det(\mathcal{M})}{M}}, \quad (16)$$

where $\text{tr}(\mathcal{M})$ is the trace of \mathcal{M} and $\det(\mathcal{M})$ is the determinant of \mathcal{M} . As for sheared galaxies, we see that the distortion is available from a direct measurement in the image plane while the magnification measurement requires to know the value of M which is related to the light distribution in the source plane, or in an unlensed reference plane. The ACF provides a new and independent way to measure δ_i and μ which does not require shape, size or photometry of individual galaxies. Furthermore, the signal to noise ratio is proportional to the number density of background galaxies, N , instead as \sqrt{N} for the standard method (see figure 2).

A description of its practical implementation and first results are given in Van Waerbeke et al. (1996a) and Van Waerbeke & Mellier (1996b). Clearly, the ACF is the most powerful technique for measuring the orientation of very weak shear as the one we expect from large-scale structures.

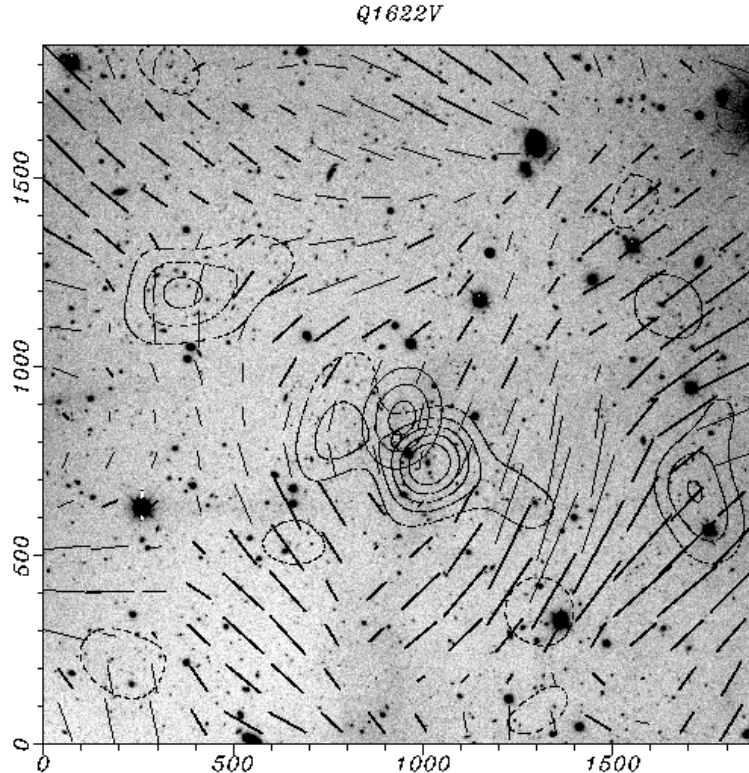


Figure 3: Shear map around the bright quasar Q1622. The image obtained at CFHT clearly shows a coherent shear. The ellipses shows the center of the shear pattern which is very close to the quasar (dark dot). The others solid lines are galaxy number isodensity contours. Clearly the quasars, the shear pattern and a galaxy concentration are almost positioned at the same place which reinforces the hypothesis of a magnification effect on the quasar.

5 The matter distribution on very large scale

The direct observation of the mass distribution on scale larger than $10 h^{-1}\text{Mpc}$ (or ≈ 1 square degree) is one of the great hopes of the weak gravitational lensing approach. Two observational directions are now being investigated. In the first one we search for the shear of dark condensation of mass that can be responsible for the magnification bias of luminous quasars and radio-sources. It probes the lumpiness of matter distribution within large-scale structures. In the second one, we analyze the statistical properties of weakly lensed background galaxies on degree scales in order to obtain constraints on the cosmological parameters and on the projected power spectrum.

5.1 Shear around radio-sources and the lumpiness of matter

Fugmann (1990) and Bartelmann & Schneider (1993a,b) have demonstrated that there is a strong correlation between the presence of galaxies or clusters and bright quasars. They interpreted this as a magnification bias induced the galaxy over-densities along the line of sight. However, the measured correlation is too strong to be only due to individual galaxies, so Bartelmann & Schneider suggested that the magnification bias originates from groups or even rich cluster of galaxies. If this suggestion is correct, the deflector responsible for the magnification bias should also induce gravitational shear onto background sources.

Bonnet et al. (1993), Mellier et al. (1994) and Van Waerbeke et al. (1996a) found a strong

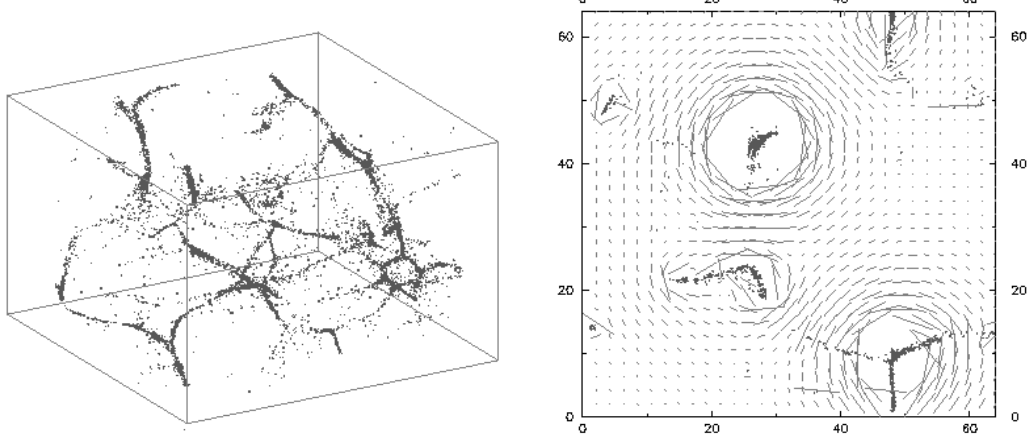


Figure 4: Simulation of shear expected from large scale structures. The left panel shows a 256^3 Mpc 3 box with dark dots indicating the location of matter. The long filaments are large scale structures which originated from a uniform distribution and an initial power spectrum $P(k) = k^{-1}$ under the adhesion approximation. The right panel shows a slice which represents the projected mass distribution as it would be observed by an observer. The thin straight lines are the local orientation and intensity of the shear. It illustrates what we expect from the future observations of weak lensing with wide field CCD.

gravitational shear and a galaxy excess around the quasar pair Q2345+007, the shear pattern being associated with a group or a small cluster. In the same way Fort et al. (1996a) have measured the shear around a few over-bright QSO-s that could be magnified by nearby lensing mass (figure 3). It is the first tentative to detect gravitational structures from a mass density criteria rather than luminosity excess. The field of view around each QSO is small and up to now, there is not enough data to draw a synthetic view of the global matter distribution. However, both weak lensing detection around bright radio-sources and the correlations found by Bartelmann & Schneider seem to favor a model where clumps of dark matter are more numerous than expected and concentrated on groups and clusters of galaxies.

5.2 Statistical analysis of shear on very large scale

In the statistical studies of the shear at very large scale the lenses are not individually identified, but viewed as a random population affecting the shape of the galaxies with an efficiency depending on their distances. Indeed, in this approach, we consider the statistical properties of the shear measured on background objects for randomly chosen line-of-sights. The measured shears are actually filtered at a given angular scale so that a signal of cosmological interest can be extracted. For a filtering scale of about one degree, the structures responsible of the gravitational shear being at a redshift of about 0.4 are expected to be on scales above $10 h^{-1}\text{Mpc}$, that is in a regime where their properties can be easily predicted with the linear or perturbation theory. Within this line of thought, Blandford et al. (1991), Miralda-Escudé (1991) and Kaiser (1992) argued that the projected power spectrum should be measurable with such a method provided shape parameters are averaged on the degree scale, as it is illustrated on figure 4.

For such a scale, however, the shear is expected to be as low as 1%. Therefore its detection requires high image quality to avoid uncontrolled errors, and large angular coverage so that it is possible to separate the gravitational shear from the intrinsic galactic ellipticities by averaging over thousands of galaxies. So far such a detection has not been completed due to these

severe constraints, but there are now projects to build very large CCD mosaic camera which could be capable of doing large deep imaging surveys. The MEGACAM project conducted by the French institutions, CEA (CE in Saclay) and INSU, the Canadian CNRC and the CFHT Corporation consists in building a $16K \times 16K$ camera at the prime focus of CFHT. This camera will provide a total field of view of $1^\circ \times 1^\circ$, with image quality lower than $0.5''$ on the whole field. Using a Perturbation Theory approach, Bernardeau et al. (1996) have analyzed the statistical properties of the gravitational shear averaged on MEGACAM scales. They have shown that with the observation of about 25 such fields, one could recover the projected power spectrum and Ω independently by using the variance and the skewness (third moment) of the one-point probability distribution function of the local convergence in the sample ¹. Basically, these moments write,

$$\langle \kappa_\theta^2 \rangle \propto P(k) \Omega^{1.5} z_s^{1.5} \quad (17)$$

and

$$\frac{\langle \kappa_\theta^3 \rangle}{\langle \kappa_\theta^2 \rangle^2} \propto \Omega^{-0.8} z_s^{-1.35} \quad (18)$$

where $\theta = 30'$ is the scale where the convergence κ is averaged, $P(k)$ is the projected power spectrum of the dark matter and z_s is the averaged redshift of sources. Note that the skewness, expressed as the ratio of the third moment by the square of the second, does not depend on $P(k)$ and provides a direct information on Ω .

These important results show that a very large-scale survey of gravitational shear can provide important cosmological results which could be compared with those coming from large-scale flows and observations of the cosmic microwave background anisotropy spectrum that are expected to culminate with the COBRAS/SAMBA satellite mission. However, there are two shortcomings that must be handled carefully: first, it requires detection of very weak shear from shape parameters of galaxies. Thus, the image quality of the survey is a crucial issue. The ACF method proposed by Van Waerbeke et al. (1996a) should provide accurate shape information with a high signal to noise ratio. It is probably the best available method for measuring shear on very large scales. The second point is the strong dependence of the variance and the skewness with the redshift of lensed sources. Since there are no hopes to obtain redshifts of these galaxies even from spectroscopy with the VLT-s, we face on a difficult and crucial problem. It may be overcome if multicolor photometric data can provide accurate redshifts for very faint galaxies. Another possible solution could be the analysis of the radial magnification bias of faint distant galaxies around rich clusters which, indeed, probes the redshift distribution of the sources (Fort et al. 1996b and see section 6).

6 Measuring the cosmological constant

One remarkable property of gravitational lensing effect is the local change of the galaxy number density. The observable number density of sources results of the competition between deflection effect which tends to enlarge the projected area and the magnification which increases the number of faint sources. The expected galaxy number density is,

$$N(r) = N_0 \mu(r)^{2.5\alpha-1}, \quad (19)$$

where μ is the magnification at the position r and $\alpha = d \log(N)/dm$ is the slope of the galaxy counts. When α is larger than 0.4, the galaxy number density increases. At faint

¹detailed calculations have shown however that there is a slight degeneracy with the cosmological constant.

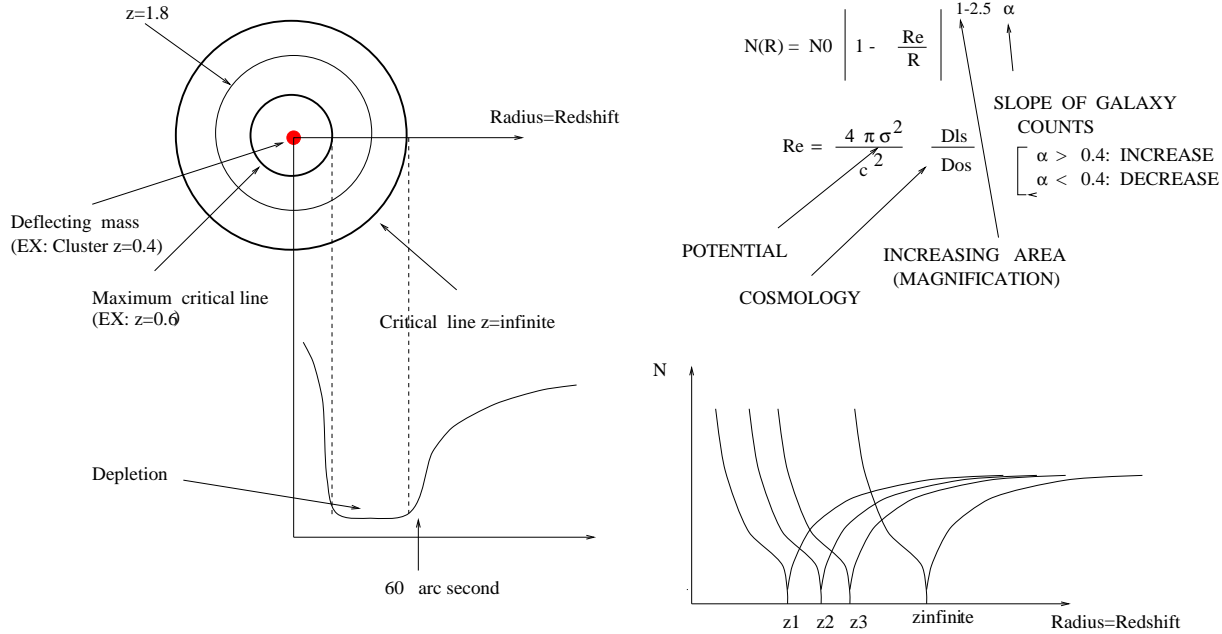


Figure 5: Principle of measurement of redshifts from depletion. The right panel shows the depletions curves expected by a singular isothermal sphere. If the lens is perfectly known the minimum of each depletion curve (right panel) depends only of the redshift of the source and the radial position of the critical line is actually equivalent to a redshift. In a realistic case, the redshift distribution is broad and the left panel shows the depletion as it would be observed: instead of the single peaked depletion we expect a more pronounced minimum between two radii (= two redshifts) whose angular positions strongly depend on the cosmological constant for high redshift sources. Thus, if the mass distribution of the lens is well known as in the rich lensing cluster Cl0024+1654, λ can be inferred from the shape of the depletion curve.

limiting magnitude, α becomes significantly smaller than 0.4 and a clear galaxy depletion can be detected (Broadhurst 1995, Fort et al. 1996b).

The shape of the depletion curves depends on the magnification μ which is a complicated function of the lensing potential, the redshift distribution of sources and the cosmology. For a singular isothermal sphere, the amplification at radius r writes,

$$\mu(r) = \frac{4\pi\sigma^2}{c^2} \frac{D_{ls}}{D_{os}} \frac{r}{r-1}, \quad (20)$$

and the depletion curve for a single redshift of sources looks like those shown in figure 5. For a redshift distribution, the depletion curve shows a plateau between two extremum points corresponding to the lowest and highest redshift of the sources. Once the redshift of one source is known, the radial position of the highest redshift strongly depends on the cosmological constant.

Fort et al. (1996b) tentatively measured depletions curves in Cl0024+1654 (see figure 6) and A370 of faint galaxies close to the noise level. With the hypothesis of a single lens along the line of sight they found that the angular position of the highest-redshift sources is very high and imposes that the most distant galaxies visible in the field have redshifts larger than 2, while the width of the depleted areas extend as far as 60 arcseconds which is incompatible with a low- λ universe. In fact, the observations provide a lower limit $\lambda > 0.6$ (figure 6).

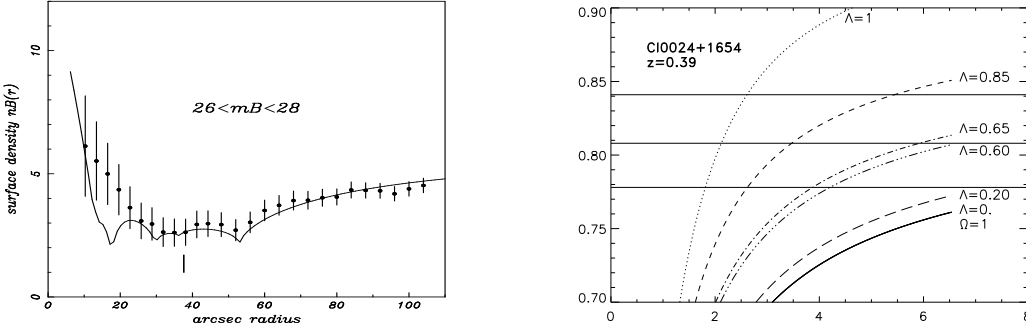


Figure 6: Measuring the cosmological constant from the depletion observed in Cl0024. The left panel shows the depletion curve observed in Cl0024+1654. From the redshift of the first minimum and the second minimum, one can constrain the cosmological constant in order to position the second minimum at its right angular position. Whatever the redshift of the most distant sources visible on the images, we see that the angular position where the depletion curve raises again imposes that $\lambda > 0.65$

7 Conclusion

In the last ten years, the gravitational lensing effects turned out to be among the most promising tools for cosmology. It is indeed a direct probe of the large-scale cosmic mass distribution and some observable quantities revealed to be extremely sensitive to the cosmological parameters. We summarize in table 3 what we learned about Ω from the mass distribution in rich clusters of galaxies and what we expect in the near future. It shows that we can hope for strong and reliable constraints on Ω and λ from the developing observational tools: we are now aiming at a determination of the cosmological parameters within 10% accuracy.

Acknowledgements. We thanks P. Schneider, for discussions and enthusiastic support. F. Bernardeau is grateful to IAP, where most of this work has been completed, for its hospitality.

8 References

Bartelmann, M., Schneider, P. (1993a) A&A 259, 413.
 Bartelmann, M., Schneider, P. (1993b) A&A 271, 421.
 Bartelmann, M. (1995) A&A 299, 661.
 Bartelmann, M., Narayan, R. (1995) ApJ 451, 60.
 Bernardeau, F., Van Waerbeke, L., Mellier, Y. (1996) in preparation
 Blandford, R.D., Saust, A.B., Brainerd, T.G., Villumsen, J.V. (1991), MNRAS, 251, 600
 Bonnet, H., Fort, B., Kneib, J-P., Mellier, Y., Soucail, G. (1993) A&A 280, L7
 Bonnet, H., Mellier, Y., Fort, B. (1994) ApJ 427, L83.
 Bonnet, H., Mellier, Y. (1995) A&A 303, 331.

MASS OF RICH CLUSTERS:

- Ω FROM ARCS ($R < 500$ KPC): 0.1 - 0.3
- Ω FROM WEAK LENSING ($R < 2.5$ MPC): 0.3 - 0.6

MAGNIFICATION BIAS (DEPLETION CURVES)

- $\Omega < 0.3$ INCOMPATIBLE WITH OBSERVATIONS
OF THE DEPLETION AT $R = 60$ "
- $\Lambda > 0.65$ (TENTATIVE)

FUTURE:

- Ω FROM EVOLUTION OF THE MASS FUNCTION
OF CLUSTERS WITH REDSHIFT
- Ω AND $P(k)$ FROM WEAK LENSING BY LARGE
SCALE STRUCTURES.

Table 3: A summary of the values of the cosmological parameters as they are inferred from gravitational lensing. They are still some uncertainties and many hopes for the future. But a real trend toward $\Omega > 0.3$ seems well established.

Broadhurst, T. (1995) SISSA preprint astro-ph/9511150.

Broadhurst, T., Taylor, A.N., Peacock, J. (1995) ApJ 438, 49.

Fahlman, G., Kaiser, N., Squires, G., Woods, D. (1994) ApJ 437, 56.

Fort, B., Prieur, J.-L., Mathez, G., Mellier, Y., Soucail, G. (1988) A&A 200, L17.

Fort, B., Mellier, Y., (1994) A&A Review 5, 239, 292.

Fort, B., Mellier, Y., Dantel-Fort, M., Bonnet, H., Kneib, J.-P. (1996a) A&A 310, 705.

Fort, B., Mellier, Y., Dantel-Fort (1996) SISSA preprint astro-ph/9606039.

Fugmann, W. (1990) A&A 240, 11.

Kaiser, N. (1992) ApJ 388, 272.

Kaiser, N. (1996) SISSA preprint astro-ph/9509019.

Kaiser, N., Squires, G. (1993) ApJ 404, 441

Kneib, J.-P., Mellier, Y., Fort, B., Mathez, G. (1993) A&A 273, 367.

Kneib, J.-P., Mellier, Y., Pelló, R., Miralda-Escudé, J., Le Borgne, J.-F., Boehringer, H., Picat, J.-P. (1995) A&A 299, 168.

Kassiola, A., Kovner, I., Fort, B. (1992) ApJ 400, 41.

Luppino, G., Kaiser, N. (1996) SISSA preprint astro-ph/9601194.

Lynds, R., Petrossian, V. (1986) BAAS 18, 1014.

Mellier, Y., Fort, B., Kneib, J.-P. (1993) ApJ 407, 33.

Mellier, Y., Dantel-Fort, M., Fort, B., Bonnet, H. (1994) A&A 289, L15.

Miralda-Escudé, J., (1991) ApJ, 370, 1.

Narayan, R., Bartelmann, M. (1996) SISSA preprint astro-ph/9606001

Pierre, M., Le Borgne, J.-F., Soucail, G., Kneib, J.-P. (1996) A&A 311, 413.

Schneider, P., Ehlers, J., Falco, E. E., (1992), *Gravitational Lenses*, Springer.

Seitz, C., Kneib, J.P., Schneider, P., Seitz, S., (1996) in press.

Seitz, C., Schneider, P., (1995) A&A 302, 9

Seitz, S., Schneider, P., (1996) A&A 305, 388

Smail, I., Ellis, R.S., Fitchett, M. (1994) MNRAS, 270, 245.

Schneider, P. (1995), A&A, 302, 639

Soucail, G., Fort, B., Mellier, Y., Picat, J.-P. (1987) A&A 172, L14.

Squires, G., Kaiser, N., Babul, A., Fahlmann, G., Woods, D., Neumann, D.M., Böhringer, H. (1996a) ApJ 461, 572.

Squires, G., Kaiser, N., Falhman, G., Babul, A., Woods, D. (1996b) SISSA preprint astro-ph/9602105.

Tyson, J.A., Fisher, P. (1995) ApJL, 349, L1.

Van Waerbeke, L., Mellier, Y., Schneider, P., Fort, B., Mathez, G. (1996a) A&A in press. SISSA preprint astro-ph/9604137.

Van Waerbeke, L., Mellier, Y. (1996b). Proceedings of the XXXIst Rencontres de Moriond, Les Arcs, France 1996. SISSA preprint astro-ph/9606100.

Wallington, S., Kochanek, C. S., Koo, D. C. (1995) ApJ 441, 58.

Walsh, D., Carswell, R.F., Weymann, R.J., (1979), Nature, 279, 381

PROGRÈS RÉCENTS EN LENTILLE GRAVITATIONNELLE

Y. Mellier^(1,4), L. Van Waerbeke⁽²⁾, F. Bernardeau⁽³⁾, B. Fort⁽⁴⁾

⁽¹⁾*Institut d'Astrophysique de Paris,*

98^{bis} Boulevard Arago,

75014 Paris, France.

⁽²⁾*Observatoire Midi Pyrénées,*

14 Av. Edouard Belin,

31400 Toulouse, France.

⁽³⁾*Service Physique Théorique,*

CE de Saclay,

91191 Gif-sur-Yvette Cedex, France.

⁽⁴⁾*Observatoire de Paris (DEMIRM),*

61 Av. de l'Observatoire,

75014 Paris, France.

Abstract

L'effet de lentille gravitationnelle est aujourd'hui considéré comme un des outils les plus prometteurs de la cosmologie. Il sonde directement la matière distribuée dans les grandes structures et peut aussi fournir des informations importantes sur les paramètres cosmologiques, Ω et Λ . Dans cet article de revue, nous résumons les progrès observationnels et théoriques récents les plus marquants obtenus dans ce domaine au cours des cinq dernières années.